mathematics

IMPACT FACTOR 2.3

CITESCORE 4.0

Article

Quantum-Fuzzy Expert Timeframe Predictor for Post-TAVR Monitoring

Lilia Tightiz and Joon Yoo

Special Issue

Advances in Quantum Computing and Applications

Edited by

Prof. Dr. Frank Phillipson, Dr. Sebastian Feld, Dr. Matthias Möller, Ward van der Schoot and Niels Neumann

MDPI

https://doi.org/10.3390/math12172625

mathematics

MDPI

Article

Quantum-Fuzzy Expert Timeframe Predictor for Post-TAVR Monitoring

Lilia Tightiz and Joon Yoo *

School of Computing, Gachon University, 1342 Seongnam-daero, Seongnam-si 13120, Republic of Korea; liliatightiz@gachon.ac.kr
* Correspondence: joon.yoo@gachon.ac.kr

Abstract: This paper presents a novel approach to predicting specific monitoring timeframes for Permanent Pacemaker Implantation (PPMI) requirements following a Transcatheter Aortic Valve Replacement (TAVR). The method combines Quantum Ant Colony Optimization (QACO) with the Adaptive Neuro-Fuzzy Inference System (ANFIS) and incorporates expert knowledge. Although this forecast is more precise, it requires a larger number of predictors to achieve this level of accuracy. Our model deploys expert-derived insights to guarantee the clinical relevance and interpretability of the predicted outcomes. Additionally, we employ quantum computing techniques to address this complex and high-dimensional problem. Through extensive assessments, we show that our quantum-enhanced model outperforms traditional methods with notable improvement in evaluation metrics, such as accuracy, precision, recall, and F1 score. Furthermore, with the integration of eXplainable AI (XAI) methods, our solution enhances the transparency and reliability of medical predictive models, hence promoting improved clinical practice decision-making. The findings highlight how quantum computing has the potential to completely transform predictive analytics in the medical field, especially when it comes to improving patient care after TAVR.

Keywords: ant colony optimization; adaptive network-based fuzzy inference system; eXplainable AI; quantum computing; transcatheter aortic valve replacement

MSC: 81Q93

Citation: Tightiz, L.; Yoo, J. Quantum-Fuzzy Expert Timeframe Predictor for Post-TAVR Monitoring. *Mathematics* **2024**, *12*, 2625. https://doi.org/10.3390/math12172625

Academic Editors: Frank Phillipson, Sebastian Feld, Matthias Möller, Ward van der Schoot and Niels Neumann

Received: 20 June 2024
Revised: 16 August 2024
Accepted: 22 August 2024
Published: 24 August 2024

1. Introduction

The procedure of severe aortic stenosis treatment has changed dramatically with the introduction of TAVR, especially for patients who pose a high surgical risk. Nonetheless, the requirement for PPMI has proven to be one of the most common post-procedural difficulties. PPMI functionality in treating cardiac rhythm complications resulting from TAVR makes it crucial both before and after the procedure. PPMI is occasionally required to maintain appropriate cardiac rhythm and function following TAVR, a minimally invasive procedure for aortic valve replacement, because it may hurt the heart's electrical system. PPMI must be taken into account to improve patient safety and outcomes, especially for patients who have pre-existing diseases that raise their likelihood of experiencing problems with their heart rhythm after TAVR. Innovative techniques that improve the accuracy of PPMI predictions are desperately needed in light of these challenges to guarantee optimal patient care and procedure results.

1.1. Motivation

With severe aortic stenosis, TAVR has become the accepted treatment of preference. It is constructive for patients undergoing high-risk surgery. Post-procedural problems, such as heart rhythm abnormalities that require PPMI, present considerable difficulties. Inadequate clinical outcomes result from the inaccuracies in the current prediction models

for PPMI post-TAVR, which often disregard patient-specific factors and intricate interdependencies between procedural variables. Furthermore, it is difficult to predict when these rhythm disturbances will manifest because they can occur anytime from right after surgery to more than 48 h later. This highlights the shortcomings of current predictive models, which frequently fail to take important procedural and patient-specific factors into account. This discovery highlights the pressing need for a more accurate and resilient forecasting technology that can adjust to the unique circumstances of each instance.

This work presents a complex quantum-fuzzy expert timeframe predictor with the help of an ANFIS and QACO. This innovative integration uses fuzzy logic systems' sophisticated reasoning, influenced by expert clinical insights, and quantum computing's capacity to process large, complicated datasets efficiently. This model seeks to improve procedural strategy optimization and patient care by increasing the specificity and accuracy of PPMI time prediction post-TAVR.

Moreover, the utilization of XAI techniques enhances our model by guaranteeing predictability and transparency, both of which are crucial for clinical decision-making. In addition to meeting the urgent need for improved forecasting tools in cardiac care after TAVR, this strategy establishes a standard for incorporating cutting-edge computational methods into clinical practice.

1.2. Related Work

Since Machine Learning (ML) provides a more precise and comprehensive analysis of patient data, it is an effective tool for forecasting PPMI necessity. Tsushima et al. [1] examined ML algorithms for predicting the necessity of PPMI following TAVR. The researchers achieved a range of model accuracies for different ML techniques, with the highest AUC of 0.693 being reached by Simple Logistic Regression (SLR)- and Locally Weighted Learner (LWL)-based models. Agasthi et al. [2] concentrated on applying Gradient Boosting Machine (GBM) models to predict the need for a PPMI after TAVR. The authors in this paper showed that these models outperformed traditional risk score models, with superior AUC values of 0.66 and 0.72 for predicting a 30-day and a 1-year post-TAVR PPMI, respectively. Truong et al. [3] demonstrated that the risk of pacemaker implantation can be predicted more accurately using the random forest model that included post-TAVR Electrocardiogram (ECG) data than using the logistic regression model or the model without post-TAVR ECG data. The RF model received scores of 0.76, 0.49, 0.18, and 0.81 for accuracy, F1 score, Brier score, and AUC, respectively. Using XGBoost for analysis, Pandey et al. [4] investigated the use of ML to predict pacemaker insertion following TAVR in patients with low Stroke Volume Index (SVI). The authors in this paper examined 288 individuals, showing an AUC of 0.702 for low SVI patients and 0.706 for normal SVI patients. To predict post-procedural PPMI following TAVR, Qi et al. [5] attempted to include pre-and post-procedural parameters. Achieving an AUROC of 0.7 in derivation and 0.71 in external validation, they identified predictors such as prior Right Bundle Branch Block (RBBB) and aortic valve area using multivariate logistic regression and Cox proportional hazard models. However, a wide range of parameters, such as patient clinical data, procedure details, and valve types, can impact the rate of post-TAVR PPMI. Additionally, unbalanced problems are the primary challenge in PPMI prediction as a dedicated issue for whole medical datasets. Imbalances frequently occur in medical datasets because certain diseases are rare or the data are scarce.

Expert expertise becomes essential in recognizing and interpreting minority classes, which are important but frequently underrepresented. During the preprocessing step, experts can significantly contribute to selecting and transforming the most relevant features for the medical context. Additionally, with their domain knowledge, experts ensure that prediction outcomes are statistically significant and medically efficient, leading to the development of more precise and clinically meaningful models. Several studies consider using statistical approaches to meta-analyze PPMI risk predictors, which are summarized in Table 1. Ref. [6] highlighted that implantation depth and Left Ventricular Outflow Tract (LVOT) calcium volume, in particular, are procedural and anatomical parameters that affect

post-TAVR PPMI rates. A comprehensive investigation by [7] identified several patient and procedural variables, including age, gender, diabetes, and valve type effects on PPMI requirements after TAVR.

Table 1. Meta-analysis studies on feature selection for PPMI requirements following TAVR diganosis.

Author & Year	Objective	Sample Size	Main Predictors
[8]	Post-procedural prediction models for PPMI with pre-existing RBBB	237	Membranous septum, First degree AVB, implantation depth
[5]	Pre- and post-procedural prediction models for PPMI	336	Prior RBBB, pre-procedural AVA, AVA ratio
[9]	Predictors for PPM after TAVR	447	Transcatheter heart valve (THV) oversizing (30 days after TAVR)
[10]	Identify predictors for PPM after TAVR	357	QRS > 120 ms, type II DM, supraventricular arrhythmias
[11]	Identify predictors for PPM after TAVR in Chinese Population	39	New-onset LBBB and lead I T wave elevation
[12]	Meta-analysis for identify predictors for PPM after TAVR	981,168	Male gender, age≥80, FDAVB, RBBB, AF, DM, CKD, Medtronic CoreValve, transfemoral TAVR, increased LVOT, and aortic annulus diameter
[13]	Meta-analysis for identify predictors for PPM after TAVR	31,261	Male gender, Mobitz Type 1 HB, Bifascicular HB, LAFB, RBBB, Mechanically-expanding, ballon expanding 29 mm
[7]	Meta-analysis for identify predictors for PPM after TAVR	71,455	Age, Male gender, DM, Baseline AV, post-procedure AV Left ventricular outflow tract calcification (left coronary cusp and non-coronary cusp), Valve size, balloon expanding, Pre-procedure balloon dilatation, Post-procedure balloon dilatation, Implantation depth
[14]	Risk predictor model for pacemaker implantation after TAVR	1071	Self-expanding valve, RBBB, pre-existing first-degree AVB
[15]	Predictors for PPM after TAVR	182	Previous RBBB and LVOT-EI
[16]	Develop risk score for pacemaker implantation post-TAVR	1266	Syncope history, baseline RBBB, QRS duration, higher degree of oversizing
[17]	Predictors for PPM after TAVR	311	High body mass index, bradycardia, RBBB
[18]	Predictive model for pacemaker implantation post-TAVR	18,400	RBBB, LBBB, bradycardia, 2nd-AVB, transformal approach
[19]	Predictive model for pacemaker implantation post-TAVR	240	RBBB, NCC-DLZ CA, MS length
[6]	Identify predictors of PPMI post-TAVR	229	RBBB, Deep valve implantation, LVOT calcification
[20]	Identify predictors of PPMI post-TAVR	1973	RBBB, the prosthesis to LV outflow tract diameter ratio and the LV end-diastolic diameter

The Emory Risk Score was created by [16] to classify patients according to their chance of requiring a pacemaker following TAVR, considering variables such as Right Bundle Branch Block and syncope history. A detailed meta-analysis by [13] confirmed the importance of baseline atrioventricular conduction delays, the type of valve prosthesis, and male sex as PPMI predictors. The current studies' shortcomings include imbalanced data and small event sizes, which hinder the utilization of various variables in the post-procedural prediction model. Researchers were forced to incorporate a limited number of

predictors because of rules such as the ten events-per-variable recommendation, keeping the number of model predictors to no more than one-tenth of the total number of events [5].

Leveraging insights from meta-analyses of PPMI risk factors indicated in Table 1, our research adopts a novel method by combining expert knowledge with ANFIS to address the issues of high-dimensional and unbalanced datasets. We control scarce events and high-dimensional data by mapping more relevant features extracted from meta-analysis studies to our dataset. Moreover, ANFIS assists in implementing if–then roles coming from expert insights for making accurate decisions [21]. While the standard ANFIS model utilizes Backpropagation (BP) to optimize parameters, there is a risk of getting stuck in local optima during the training phase. Deployment of evolutionary algorithms such as Particle Swarm Optimization (PSO) [22], Ant Colony Optimization (ACO) [23], Black Widow Optimization Algorithm (BWOA) [24,25], and Genetic Algorithm (GA) [26] enhance the parameter optimization of the membership functions in ANFIS.

Additionally, the time for PPMI following TAVR can vary from immediately after operation to more than 48 h, depending on the variable onset of conduction anomaly occurrence following TAVR [27,28]. Precisely estimating the need for a PPMI also enables improved resource allocation and budgetary planning, resulting in more economical healthcare provision [29]. Post-TAVR patient clinical data and time estimation for the prediction of PPMI is rarely considered in the literature. However, deploying all pre- and post-features, even when applying expert-knowledge-based methods to control dimensionality over effective features, will increase the dimension of ANFIS inputs and outputs, thereby increasing the ACO complexity. However, deploying all pre- and post-features, even when applying expert knowledge-based methods to control dimensionality over effective features, will increase the dimension of ANFIS inputs and outputs. Therefore, the ACO framework's modeling procedure becomes more difficult as an ANFIS parameter estimator. Utilizing the concepts of superposition and entanglement, quantum computing provides a way to process data exponentially faster than traditional computing techniques. Quantum computing facilitates the simultaneous analysis of several possible solutions in the context of ACO-ANFIS for PPMI prediction, greatly accelerating the membership function parameter optimization in ANFIS. This is important due to various individuals having different time windows for successful PPMI after TAVR, and it affects real-time health monitoring and decision-making. Recently, Quantum Machine Learning (QML) has offered essential computational advantages to overcome high-dimensional data challenges in healthcare systems [30]. Quantum computing provides a way to process data tenfold more quickly than traditional computing techniques by utilizing the concepts of superposition and entanglement. Therefore, in this paper, we deploy quantum computing over ACO to enhance the probability of the next node selection in our high-dimensional ACO algorithm training iterations.

Furthermore, even while earlier research has shown that ML models can identify PPMI with high predictive accuracy, it frequently fails to offer clear justifications for the models' success, such as the importance and interaction of contributing features. XAI is required in the context of our work since medical decision-making procedures depend heavily on openness and trust. Our approach aims to improve the accuracy of our model by using the Shapley Additive exPlanation (SHAP) and Local Interpretable Model-agnostic Explanations (LIME) libraries of XAI. These plots depict how specific features affect the model's predictions, allowing us to estimate the effectiveness of different features in our knowledge transfer approach. By deploying XAI, we can bridge the gap in our understanding and identify the features that are most effective in improving the model's performance. Therefore, the method helps stakeholders and doctors understand how the model works and ensures that decisions are trustworthy and based on comprehensible information. Moreover, XAI helps to check our knowledge expertise, and the QACO-ANFIS method could make the model smarter by emphasizing important predictors and how they interact.

The main problems that make it challenging to forecast the PPMI requirement after TAVR can be summarized as follows:

- Timing Variability: Patients differ significantly in when they need PPMI. After TAVR, some patients could need treatment right away, while others might experience symptoms that need PPMI a few days later. Because of this unpredictability, standardizing predictions becomes more difficult because the models must be sensitive enough to cover a large temporal range.
- Complexity of Patient Data: Every patient has a different set of factors to consider, including underlying medical issues, body reactions to TAVR, and individual recovery paths. Predictive mistakes result from current models' frequent inability to completely integrate and analyze these intricate datasets.
- Current Predictive Model Limitations: A lot of the predictive models that are now in use are limited by the following:
    - Data Simplification: A major information loss occurs when models oversimplify multidimensional, complex patient data.
    - Lack of Dynamism: In the crucial hours and days that follow TAVR, they frequently fail to take into account the dynamic changes in patient status.
    - Inadequate Integration of Clinical Expertise: Current models frequently fall short of incorporating the clinical knowledge required to properly analyze patient data.

These difficulties underline the requirement for a predictive model that not only takes these complexities into account but also adjusts to each patient's unique demands, guaranteeing prompt and precise forecasts to maximize post-TAVR treatment.

1.3. Contributions

The contributions of the paper are as follows:

- Providing the time-based prediction architecture for PPMI requirement diagnosis following TAVR.
- Improving feature selection by incorporating expert knowledge to concentrate on more relevant predictors for results that are more accurate and understandable.
- Utilizing quantum computing to enhance high-dimensional data processing in PPMI requirement diagnosis following TAVR.
- Prompt healthcare decision-making provision by employing quantum algorithms for the ACO-ANFIS framework to increase prediction model accuracy and real-time performance.
- Developing model explainability using XAI, which sheds light on feature importance and interactions and meets the requirement for transparency in AI applications in the healthcare industry.

1.4. Paper Structure

The remainder of this paper is organized as follows. Section 2 explains the used QACO-ANFIS approach and its algorithm. The results and discussion are presented in Section 3. This section also addresses the difficulties and barriers of our strategy and possible future approaches. This paper comes to a close in Section 4.

2. Proposed Method

This section describes our approach, illustrated in Figure 1. It demonstrates how the ANFIS feature selection process is guided by expert knowledge from an extensive analysis of the pertinent literature and insights from system design. The ANFIS's membership and consequence parameters are adjusted using evolutionary algorithms like ACO, GA, BWO, and PSO. This improves our model's capacity to plan patient monitoring precisely following TAVR. This section also describes the integration of quantum computing techniques to improve the performance of these algorithms, enabling faster and more efficient parameter optimization. More specific elements and how they work together are explained in the following subsections.

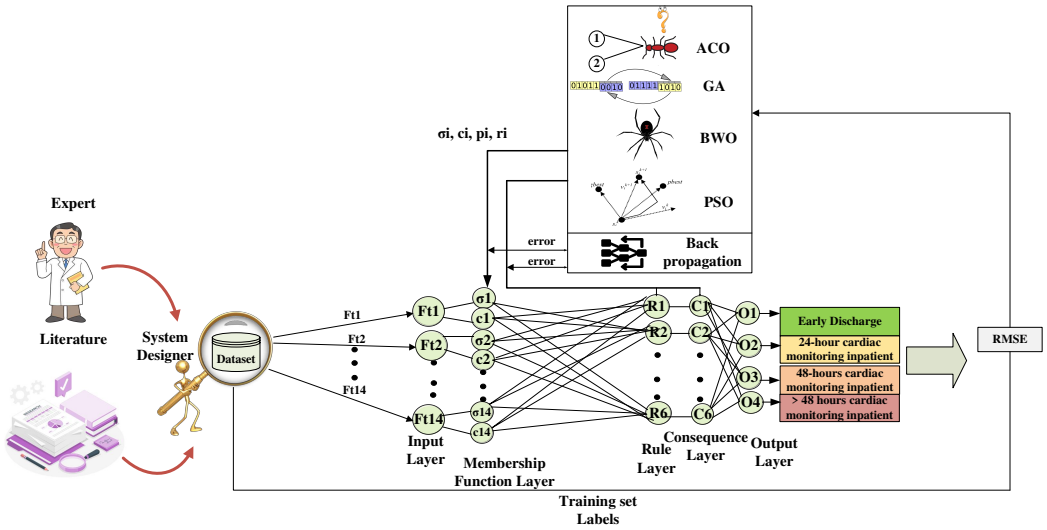

Figure 1. An overview of the system.

2.1. ANFIS Integrated with Classical ACO

The ANFIS is an artificial neural network that utilizes the Takagi–Sugeno fuzzy inference system. The approach aims to incorporate neural networks and fuzzy logic into a single framework that can benefit from both. Because ANFIS can approximate nonlinear functions, it is a popular tool for modeling complex systems and pattern recognition [31]. There are five layers in the ANFIS architecture. The first layer is called the fuzzification layer. This layer determines the membership functions that belong to the input values. In estimating membership grade, Gaussian membership functions are commonly used, as follows:

$$O_i^1 = \mu_{Ai}(x) = \exp\left(-\frac{(x-c_i)^2}{2\sigma_i^2}\right), \tag{1}$$

where the variables σ_i and c_i, respectively, represent the width and center of the Gaussian curve.

Every node in the second layer, known as the product layer, multiplies the incoming signals to generate the product. The following is the output of a node that obtains $\mu_{Ai}(x)$ and $\mu_{Bi}(y)$, where A and B are the system's inputs:

$$O_i^2 = \omega_i = \mu_{Ai}(x) \cdot \mu_{Bi}(y), \tag{2}$$

where a rule's firing strength is denoted by ω_i.

In the third layer, called the normalization layer, every node determines the ratio between the firing strength of the ith rule and the total firing strength of all the rules:

$$O_i^3 = \bar{\omega}_i = \frac{\omega_i}{\sum_j \omega_j}. \tag{3}$$

Layer 4 has the responsibility of defuzzification. The nodes in this layer have adaptive functions represented by (4).

$$O_i^4 = \bar{\omega}_i f_i = \bar{\omega}_i(p_i x + q_i y + r_i), \tag{4}$$

where f_i is a linear function of the inputs, and p_i, q_i, and r_i are the consequence parameters set. The last layer, the summation layer, consists of a single node that sums up all incoming signals to determine the total output.

$$O^5 = f = \sum_i \bar{\omega}_i f_i. \tag{5}$$

The ANFIS parameters, which include the premise parameters in the fuzzification layer and the consequent parameters in the defuzzification layer, are acquired through a hybrid learning algorithm. This algorithm combines Least Squares Estimation (LSE) and the gradient descent technique. The premise parameters are set during the forward pass, but the fixed parameters are identified using the least squares estimate. The gradient descent method updates the premise parameters throughout the backward pass while the consequent parameters remain unchanged. However, due to potential drawbacks, including slow convergence, the possibility of converging to local minima, and inefficiency in handling complicated, non-linear systems, conventional techniques like the gradient method and LSE might not be the best for ANFIS parameter adjustment. Evolutionary algorithms are the prominent alternatives to fine-tuning fuzzy systems because of their ability to perform global searches, manage complex optimization landscapes, and ultimately enhance model accuracy and performance.

ACO is an evolutionary algorithm that deploys biological inspiration to address optimization issues. It finds the most immediate routes between food sources and their nest by imitating the ant's pheromone trail-laying and trail-following behavior. The pheromone deposit is one of the main elements of this algorithm. Ants leave behind a chemical known as pheromone, which influences other ants' decisions on which path to take. Based on the quantity of pheromones and the path's visibility, ants select their routes probabilistically. The likelihood that ant k will select node j as the subsequent node from node i is provided by the following:

$$P_{ij}^{k} = \frac{[\tau_{ij}]^{\alpha} \cdot [\eta_{ij}]^{\beta}}{\sum_{l \in allowed_k} ([\tau_{il}]^{\alpha} \cdot [\eta_{il}]^{\beta})}, \tag{6}$$

where τ_{ij} is the pheromone quantity on the path from i to j, η_{ij} is the visibility, $allowed_k$ is the set of nodes that ant k can visit next, and α and β are parameters controlling the influence of pheromone and visibility, respectively.

The pheromone trails are updated with new information whenever every ant has finished traveling. Such a process of actualization is of crucial importance for guiding the subsequent choices of ants by adapting the pheromone concentration within the paths. Therefore, to prevent the solution from settling on a local optimum and for a dynamic exploration of the paths, the pheromone level is updated in two ways:

- Evaporation: The existing pheromone level on each path is reduced by applying a factor of $(1 - \rho)$, where ρ is the coefficient of evaporation of the pheromone. This weakening, in turn, reduces the level of the pheromone, and with time, the effect of a previously visited path weakens accordingly. This helps prevent the algorithm from becoming prematurely locked into a potentially suboptimal state.
- Ant Pheromone Deposits: Upon evaporation, the pheromone concentration is increased based on the pheromones deposited by the ants during their travels. More pheromone $\Delta\tau_{ij}^{(k)}$ is precisely added by each ant k to the path that connects node i to node j. An ant's experience with a trail determines the quality of this pheromone deposit. The overall pheromone level increase on this path sums up all the contributions from the ants, calculated as follows:

$$\tau_{ij} = (1 - \rho) \cdot \tau_{ij} + \sum_{k=1}^{m} \Delta\tau_{ij}^{(k)}, \tag{7}$$

  where m is the total number of ants, and $\Delta\tau_{ij}^{(k)}$ measures the pheromone that the k-th ant deposits on the path from i to j.

ACO has a sequential manner of finding the best solution. Therefore, as the number of examined routes and the number of iterations needed to achieve efficient results rise, the complexity of ACO increases significantly. Despite its usefulness, the ACO has limita-

tions, particularly when applied to complex optimization problems such as the parameter optimization of ANFIS, which involves many input features.

2.2. Quantum Entanglement Enhancement for ANFIS-ACO

Classical ACO can be slow since it selects the next node based on a pseudorandom integer and computes cumulative probabilities for each neighbor, especially when there are a lot of nodes. Due to the number of effective predictors for patient status determination after TAVR, this procedure creates a significant bottleneck in obtaining real-time solutions by utilizing ACO-ANFIS.

Currently, there is a growing interest in utilizing quantum parallelization and entanglement in quantum states to reduce the computational complexity of iterative-based optimization techniques. Superposition, the underlying parallelism of quantum computing, can greatly accelerate this procedure. By using qubits ($|\Psi\rangle$), which, in contrast to classical bits, may exist in states of superposition ($|0\rangle$ and $|1\rangle$ concurrently), quantum computing enhances problem-solving. Qubits can encode and process several paths for solving problems simultaneously with the help of superposition. Qubits are linked by entanglement as a phenomenon in which qubits interact, and regardless of distance, one's state instantly affects another. Quantum gates are used to leverage superposition and entanglement concepts. They are crucial to quantum computing because they can change the states of qubits. Quantum gates use quantum mechanics laws to work on qubits, allowing for complex computations through entanglement and superposition, in contrast to traditional logic gates, which carry out binary operations. These gates enable quantum algorithms to carry out operations that are not practical for classical computers, like the CNOT gate for entangling qubits or rotation gates $R_y(\theta_i)$ for the rotation by angle around the Y-axis [32]. With the contribution of ACO and quantum concepts, all probabilities can be processed simultaneously in a single quantum circuit execution. In addition to speeding up the calculation, this feature allows the next node to be chosen via actual randomization rather than pseudorandom numbers. Therefore, the quantum technique removes the bottleneck that hinders next-node selection, leading to faster and more efficient convergence to optimal or near-optimal solutions.

Instead of transferring all parameters directly to a quantum framework, we utilized a quantum picker in this study to optimize ANFIS parameters, following the QACO approach proposed by [33] and detailed in Algorithm 1 as follows.

Algorithm 1 Enhanced HQACO for ANFIS Parameter Optimization integrated with Quantum Circuit Generation

INITIALIZATION
Initialize pheromone levels $\tau_{i,j}$ for all edges i, j in the ANFIS parameters graph. Set hyperparameters α, β, and ρ. Determine quantum register size q accordingly, and initialize classical registers $C1$, $C2$, $C3$.
for each $ant \in \{1, \ldots, k\}$ **do**
  Select the start node with equal probability.
  for each parameter type $\in [MFi, MFo]$ **do**
    Calculate transition probabilities.
    Call: $ProbabilityToAngleMapping(P)$.
    Call: $GenerateQuantumCircuit(R)$.
    Perform quantum measurement and update $next\_parameter\_set$.
    Update classical registers $C1$, $C2$, $C3$ with current state, decision, and probabilities.
    Update ANFIS model parameters based on quantum decisions.
    Evaluate ANFIS model performance and update pheromones.
  end for
end for
Apply the best parameters to the ANFIS model.
Check termination conditions.
return optimized ANFIS parameters.

Algorithm 1 *Cont.*

FUNCTION PROBABILITYTOANGLEMAPPING(P)
Require: Array of probabilities P_i with $2^{num_{qubits}}$ dimension.
Ensure: Array of spherical angles $\phi = \{\phi_1, \phi_2, \ldots, \phi_{n-1}\}$.
Initialize an empty array ϕ for the spherical angles.
for $i = 1$ to $num_{qubits} - 1$ **do**
if $P_i = 0$ **then**
Add 0 to ϕ.
Populate the remaining entries of ϕ with π.
Exit the loop.
else
$\phi_i = 2 \times \arcsin^{-1}(\sqrt{P_i})$.
$\forall P_i \in P, P_i / \sin(\phi_i/2)$.
end if
end for
return ϕ.

FUNCTION GENERATEQUANTUMCIRCUIT(R)
Require: Array of spherical angles ϕ.
Ensure: Quantum circuit QC.
Determine the number of qubits *num_qubits* based on the length of $\phi + 1$.
Initialize a quantum circuit QC with *num_qubits*.
if *num_qubits* > 2 **then**
Decompose A into two parts for G1 and G2 circuits, respectively.
Generate G1 using the first $(2^{num\_qubits-1} - 1)$ angles from ϕ.
Apply a multi-controlled R_y gate using the $(2^{num_qubits-1})$th angle.
Apply $(num\_qubits - 1)$ CNOT gates, each controlled by the *num_qubits*th qubit.
Generate G2 using the last $(2^{num\_qubits-1} - 1)$ angles from ϕ.
else
Apply sequence of R_y and CNOT gates based on angles in ϕ.
end if
Add measurement gates to all qubits.
return QC.

- Quantum Circuit Setup: The quantum circuit is configured primarily using the GENERATEQUANTUMCIRCUIT(R) function from Algorithm 1. This function takes a set of probabilities and turns them into quantum angles that specify how the qubits are arranged in the circuit. These probabilities, which are represented by the symbol P_{ij} in Equation (6), stand for the possibility of moving from node i to node j. They are called simply P_i in the PROBABILITYTOANGLEMAPPING(P) function, assuming a serial indexing that captures all node transitions.
- The role of classical registers
  - The C1 (System State Register) contains the node status and operational flags that direct the quantum computations, as well as the present state of the system.
  - Decision variables and the probabilities connected to each decision are stored in the C2 (Decision and Probability Register), which has a direct impact on updates and modifications made to the ANFIS model parameters in response to results from the quantum circuit.
  - The parameter adjustment register, or C3, keeps track of the changes made to the ANFIS parameters after quantum computation, making sure that the model's tuning appropriately incorporates the feedback from the quantum measurements.
- Probability to Angle Conversion: The process of converting these probabilities into angles that quantum gates can use is handled by the function PROBABILITYTOANGLEMAPPING(P). The procedure entails the following:

- The angle is set to 0, and succeeding entries are filled with P_i, thereby nullifying those pathways in the quantum computation if $P_i = 0$, signifying an impractical path.
- In the case of non-zero probabilities, $2 \times \arcsin^{-1}(\sqrt{P_i})$ will determine the angle ϕ_i, assigning a corresponding quantum state angle to every likelihood.

- Quantum Decision-Making: The quantum state $|\Psi\rangle$ is initialized to reflect all possible paths weighted by their estimated probabilities when the quantum circuit is set up. This quantum state collapses upon measurement to a basis state $|i\rangle$, which represents the path selected according to quantum probability. Real-time optimization is made possible by this selection, which is not only faster than the classical approach but also more accurate.
- Feedback and Optimization: The quantum measurement results have a direct bearing on the ANFIS parameter adjustments. Figure 2 illustrates this real-time feedback loop, which continuously fine-tunes the model to guarantee ideal parameter settings, improving the patient monitoring system's accuracy and effectiveness.

2.3. ANFIS Arrangement for Using QACO

The ANFIS model graph must be arranged by the post-TAVR treatment prediction model to apply QACO, and the qubit count must be ascertained [34]. As shown in Table 2, our model configuration processes fourteen binary input features that are essential for determining the patient's state after TAVR. These inputs are crucial for guiding the clinical decision-making process and are chosen after expert consultations and considering meta-analysis studies represented in Table 1. Gaussian membership functions are linked to every input characteristic, and QACO dynamically optimizes their parameters to precisely capture the diagnostic ambiguities that are common in clinical situations.

Decisions such as "Early Discharge", "24 h Inpatient Monitoring", "48 h Inpatient Monitoring", and ">48 h Monitoring" determine the ANFIS model's final results. Six fuzzy logic rules, each methodically derived from significant features as listed in Table 2, define these outputs. These rules cover a variety of scenarios based on several cardiac and demographic variables, converting the processed input features into actionable clinical decisions. These guidelines, which are separate yet connected, guarantee that patient treatment plans are managed thoroughly after TAVR, thereby meeting all possible patient situations. In our method, the ANFIS graph is arranged by mapping sets of input and output parameters of the ANFIS framework as input (MFi) and output (MFo) vectors, as delineated in Figure 3. The input vector $\vec{ft}$ is given two Gaussian membership functions, μ and c, which help the model sense subtle variability in the data, which is closely related to the clinical regime of TAVR presented. Furthermore, each attribute in these vectors relates to some parameter of premises p, q that is integrated with the parameters of rules r, discretely resulting in complex output membership functions. As shown in Figure 3, the ANFIS architecture consists of 52 nodes with a connectivity of up to 6 (G_d). These metrics allow us to calculate the required qubit number as follows:

$$num_{qubits} = max(log_2(G_n), log_2(Max_{G_d}) = 6. \quad (8)$$

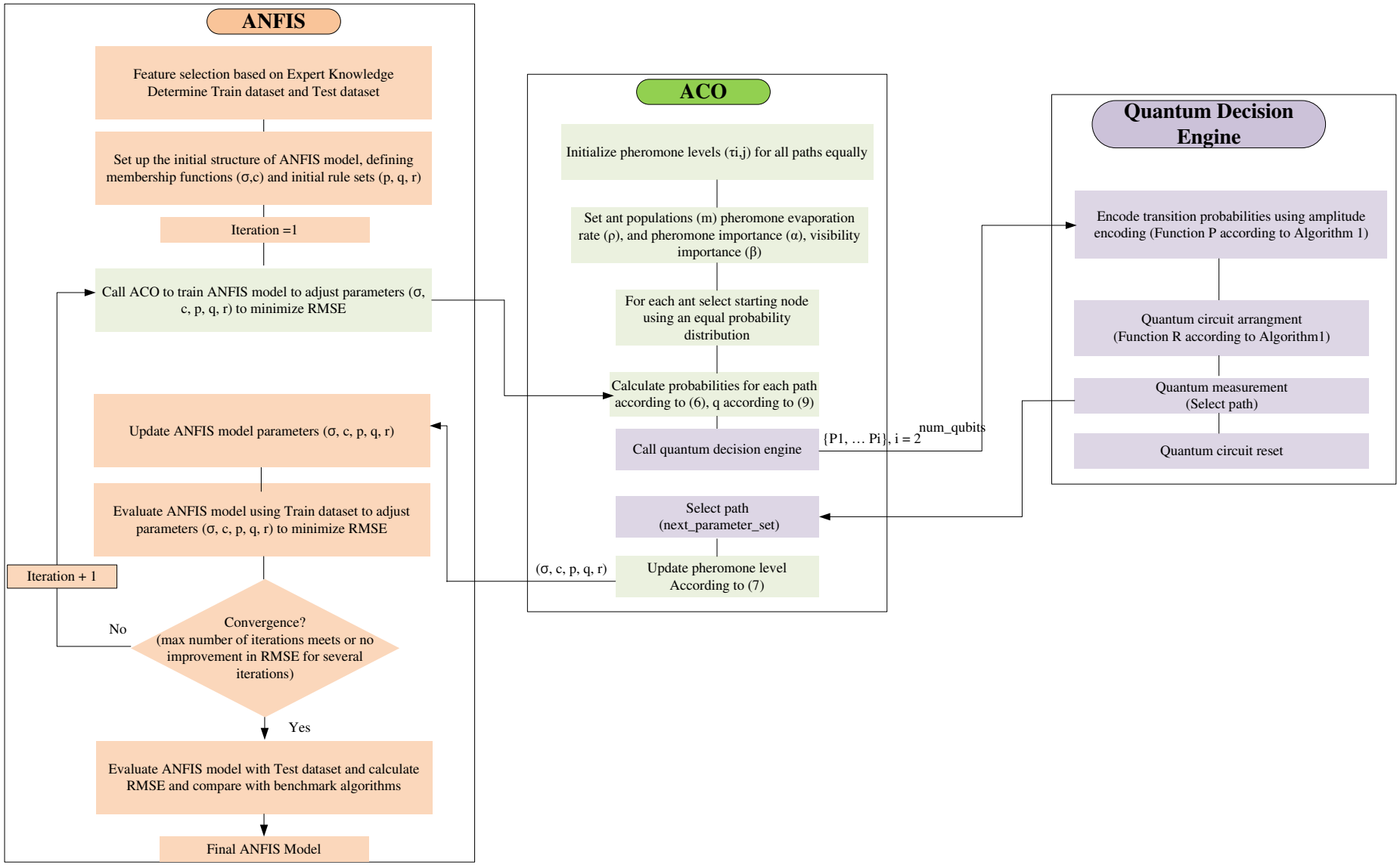

Figure 2. Flowchart of the ANFIS parameter optimization process via quantum-enhanced ACO for TAVR outcome prediction.

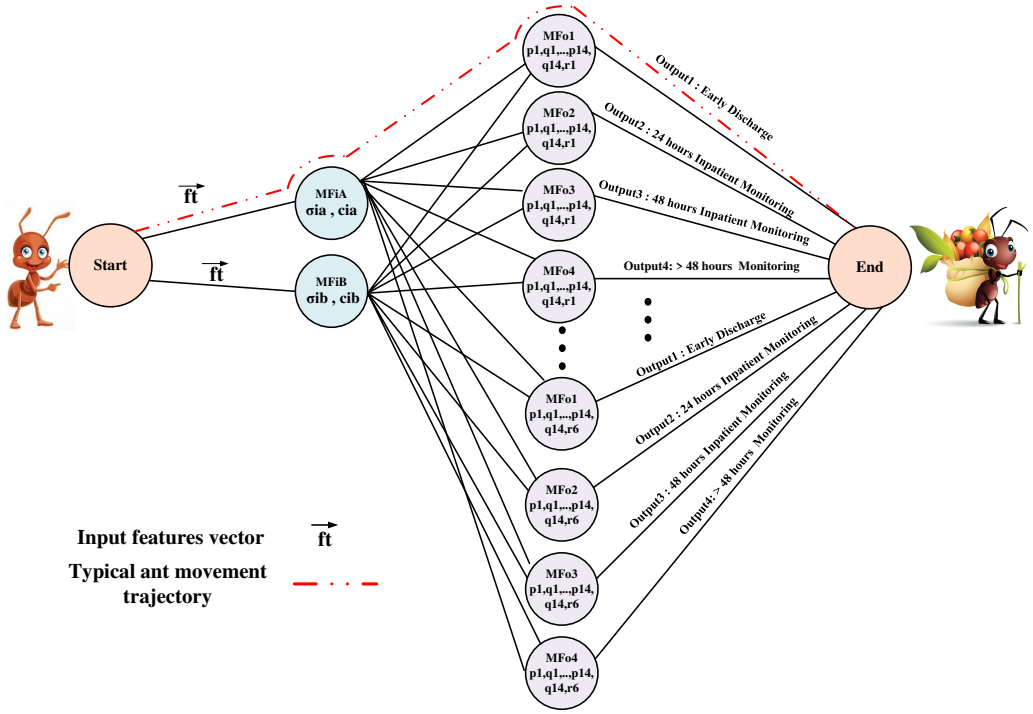

Figure 3. Graph overview of customized ANFIS-ACO network for enhanced PPMI prediction post-TAVR.

Table 2. Effective decision-making features for post-TAVR monitoring and management.

Input		Output	
No.	**Feature**	**No.**	**Decision**
1	ft1: No Baseline RBBB ft2: Absence of New ECG Changes	1	Early Discharge
2	ft3: Baseline RBBB ft4: Baseline LBBB ft5: New-onset RBBB ft6: New-onset LBBB ft7: post balloon dilatation ft8: 130 ms < QRS < 160 ms ft9: Prolongation of PR > 20 ms	2	24 h Inpatient Monitoring
3	ft3: Baseline RBBB ft4: Baseline LBBB ft5: New-onset RBBB ft6: New-onset LBBB ft7: post balloon dilatation ft10: QRS>160 ms	3	48 h Inpatient Monitoring
4	ft11: Baseline Hypertension ft4: Baseline RBBB ft12: Diabetes mellitus ft13: Male sex f14: Age	4	>48 h monitoring

It guides the selection and calibration of model inputs and the formulation of decision rules by insights from meta-analysis and the expert literature identified in Table 1. These inputs are linked explicitly in Table 2 to specific impacts on decision outputs in a structured and empirically supported way for our model.

3. Results and Discussion

3.1. Experimental Setup

Our experiment was carried out on a PC running 64-bit Ubuntu 24.04 (Linux) with an Intel(R) Core(TM) i3-7100 CPU running at 3.90 GHz and 16.00 GB of RAM. We applied the Qiskit programming framework to the quantum probabilistic provisioning. Table 3 represents the hyperparameters of the proposed methods and benchmark algorithms. The used dataset was provided by [35], including pre- and post-TAVR ECG, procedure, laboratory, and clinical data of patients who had undergone TAVR.

Table 3. Summary of hyperparameters for various methods.

Method	Key Hyperparameters	Value
ANFIS	MFi Type	Gaussian (μ&c)
	No. of MFi	2
	MFo	Linear
	No of Fuzzy rules	6
ACO	No. of Ants	1000
	Weight of pheromone on decision α	0.4
	Weight of heuristic data on decision β	0.6
	Evaporation of pheromone per step	0.05
	Max of iteration	1000
GA	population size	100
	Mutation rate	0.5
	Crossover rate	0.8
	Selection intensity	0.5
	Max of iteration	1000
BWO	population size	500
	Procreation rate	0.8
	Mutation rate	0.7
	Cannibalism rate	0.6
	Max of iteration	1000
PSO	population size	100
	Cognitive parameter	1.5
	Social Parameter	1.5
	Min of inertia weight	0.4
	Max of inertia weight	0.9
	Max of iteration	1000

3.2. Experimental Experience Results and Discussions

Table 4 represents the performance metrics for various ANFIS methods based on evaluations from both the training and test data sets. The traditional ANFIS-BP and evolutionary-based ANFIS parameter estimation, such as ANFIS-GA, ANFIS-PSO, ANFIS-BWOA, ANFIS-ACO, and ANFIS-QACO, are measured using the following metrics: accuracy, precision, recall, and F1-score.

Table 4. Benchmark algorithms performance evaluation on training and testing dataset.

	Train Dataset				Test Dataset			
Metrics / Method	Accuracy	Precision	Recall	F1-Score	Accuracy	Precision	Recall	F1-Score
ANFIS-BP	0.68	0.73	0.7	0.71	0.67	0.72	0.7	0.71
ANFIS-GA	0.85	0.80	0.83	0.86	0.82	0.81	0.8	0.86
ANFIS-PSO	0.82	0.8	0.81	0.79	0.8	0.81	0.83	0.85
ANFIS-ACO	0.85	0.85	0.8	0.85	0.83	0.81	0.82	0.81
ANFIS-BWOA	0.89	0.88	0.89	0.89	0.9	0.90	0.90	0.89
ANFIS-QACO	0.99	0.97	0.96	0.97	0.97	0.96	0.97	0.96

Based on both datasets, ANFIS-QACO performs better than other approaches in every statistic, as shown in the table. ANFIS-QACO achieves the highest accuracy (0.99), precision

(0.97), recall (0.96), and F1-score (0.97) on the training dataset specifically. In a similar vein, it continues to lead the test dataset with the greatest F1-score (0.96), accuracy (0.97), precision (0.96), and recall (0.97). Additionally, the QACO-ANFIS model is more effective in classifying true positive rates at different threshold values, according to Figure 4a. QACO-based ANFIS executes better in terms of ROC-AUC of 0.96 and outperforms other methods, including standard BWO (0.89), ACO (0.87), GA (0.84), PSO (0.8), and ANFIS-BP (0.71). Figure 4b illustrates how different ANFIS models behave concerning convergence during training, as determined by the root mean square error (RMSE) during multiple iterations. The RMSE approaches near zero after 120 iterations for the QACO-ANFIS model, indicating faster learning and adaptability. This illustrates how parallelism with superposition leads to rapid and efficient convergence of the model. On the other hand, slower convergence and larger RMSE indicate less efficient learning in other models, including ANFIS-ACO, ANFIS-BWO, ANFIS-GA, ANFIS-PSO, and ANFIS-BP.

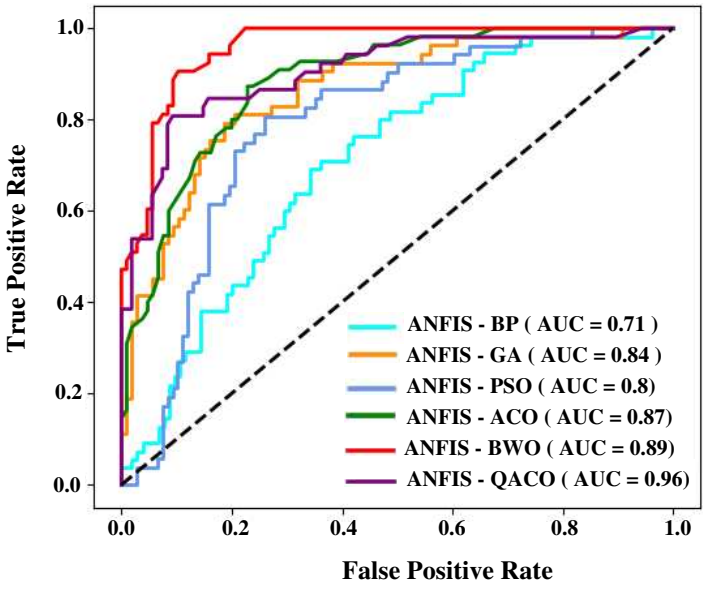

(**a**)

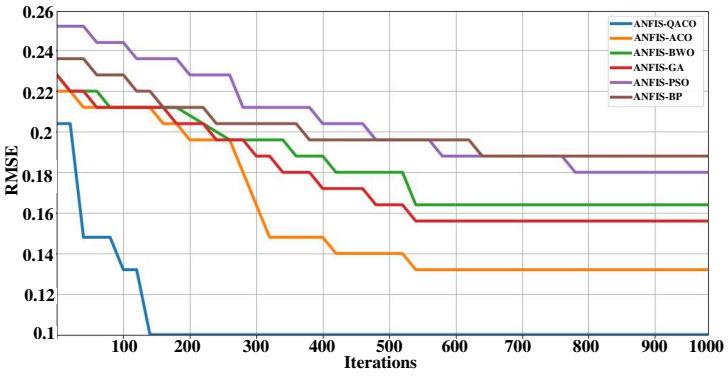

(**b**)

Figure 4. Benchmark model performance AUC evaluation comparison and convergence performance. (**a**) ROC curve and ROC-AUC of benchmark ML algorithms on test dataset. (**b**) Benchmark algorithms training convergence based on RMSE in each iteration.

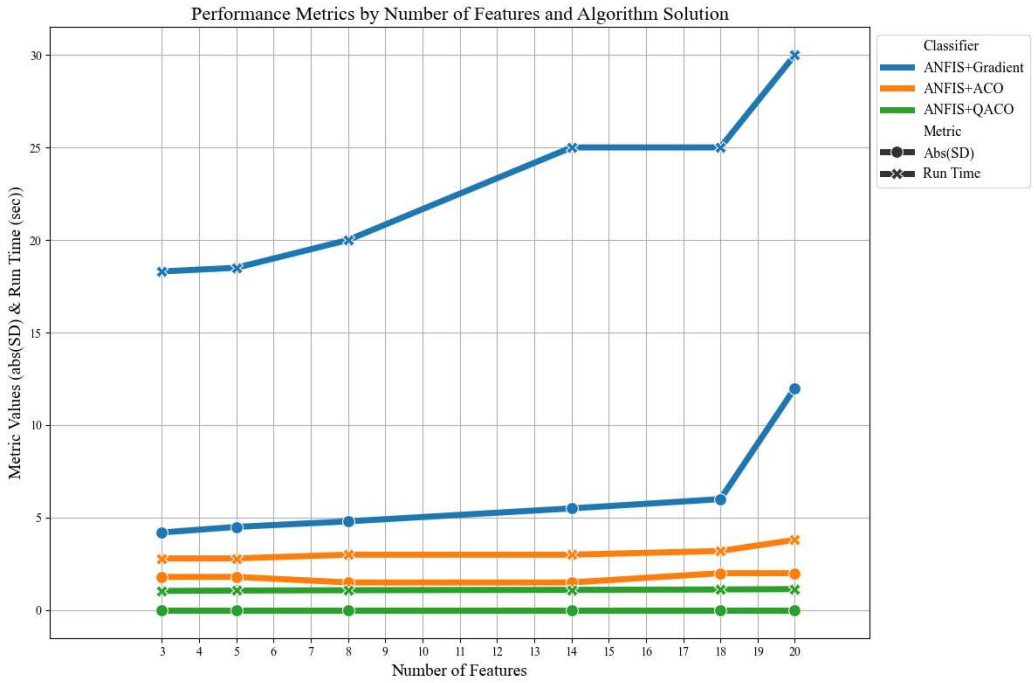

Figure 5. Run time and SD of benchmark algorithms with different number of features.

We ran our technique 100 times with different feature counts to evaluate accuracy deviations and runtime. Comparing QACO's stability in improving ANFIS versus conventional evolutionary algorithms, Figure 5 and its detailed information represented in Table 5 show the effectiveness of a quantum-based solution in providing a stable solution. Remarkably, ANFIS-QACO runs far faster than ANFIS-BP, taking only a tenth of the time. The parallelism power of qubits minimizes the impact of added features on runtime.

Table 5. Benchmark algorithm performance with different number of features.

Method \ No of Features	3	5	8	14	18	20
ANFIS + Gradient—Abs(SD)	4.2	4.5	4.8	5.5	6	12
ANFIS + ACO—Abs(SD)	1.8	1.8	1.5	1.5	2	2
ANFIS + QACO —Abs(SD)	0.0	0.0	0.0	0.0	0.0	0.0
ANFIS + Gradient—Run Time	18.3	18.5	20	25	25	30
ANFIS + ACO —Run Time	2.8	2.8	3	3	3.2	3.8
ANFIS + QACO —Run Time	1.04	1.06	1.08	1.10	1.12	1.14

We developed our model through simulation by Qiskit package deployment, which runs in a noise-free environment. It is important to note, however, that the noise and errors inherent in Noisy Intermediate-Scale Quantum (NISQ) systems limit the complexity and precision of their computations. As the number of features and qubits increases, NISQ systems can run just up to seven qubits efficiently, preserving accuracy while reducing computational time. However, NISQ performance could deteriorate as the qubit count and dataset dimensions increase [36]. Our method results are compatible with real-world quantum settings and simulations using six qubits. Additionally, in contrast to conventional sequential analysis, our suggested approach deploys quantum principles for node selection in ACO, enabling the evaluation of all node probabilities concurrently. The effectiveness of our model is ensured by this quantum computation method in conjunction with traditional arithmetic processing on classical machines. Therefore, with an increasing number of anticipated qubits, our approach still provides an accurate and stable solution. However, we plan to implement our scenario in the NISQ environment, utilizing the IBM Quantum Experience cloud computing environment, in the future.

The fuzzy system, after training, provides interpretable outputs for clinicians. The trained ANFIS model uses Gaussian membership functions for feature inputs such as "No Baseline RBBB" and "Age", as shown in Figure 6. Figure 6a represents the membership functions for "Baseline RBBB". The crossing curves for the "Yes" and "No" states, in red and blue, respectively, model a fuzzy boundary between the classes due to possible clinical data uncertainty leading to a Baseline RBBB diagnosis. In essence, this crossing corresponds to a transition zone beyond which neither classification is complete and, hence, models the inherent ambiguity in a medical diagnostic process.

Figure 6b shows the fuzzy membership functions for the input "Age". The green curve ("Below 80") and the blue curve ("80 and Above") are built around the shifting risk profile with age. The green curve peaks around 70 years but is very broad, reflecting the gradual increase in risk with age. The peak at 70 indicates that the risk surges at this age but remains moderate. The blue curve, peaked at 80 years, stands for a sharper increase in risk—higher prudent concerns for Permanent Pacemaker Implantation in these older demographics. It provides two risk categories, enhancing nuanced decision-making and making age-based clinical interventions tailored to predicted risk levels associated with PPI.

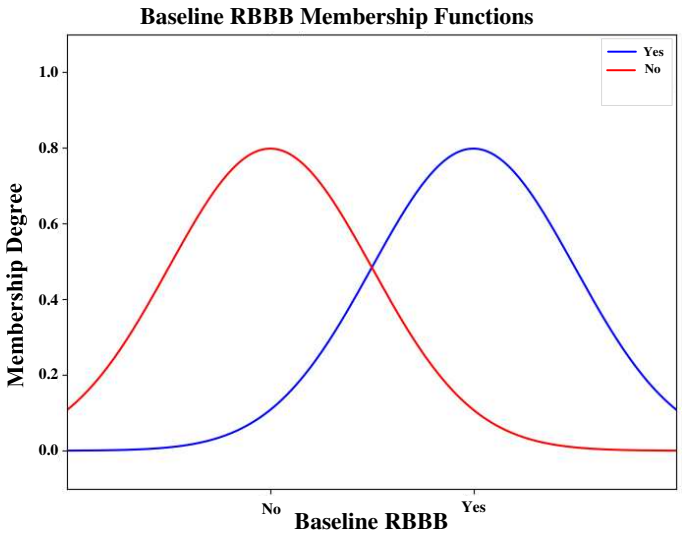

(**a**)

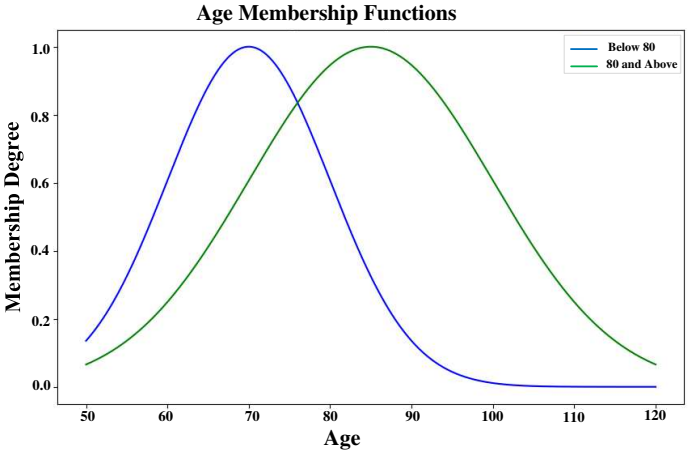

(**b**)

Figure 6. Membership degree for baseline RBBB and age in the trained ANFIS Model. (**a**) Membership degree for baseline RBBB. (**b**) Membership degree for age.

The trained ANFIS model yields these membership functions and the resulting rules consistent with the expert-driven insights enumerated in Table 2. The rules derived include the following:

Rule 1: Early Discharge
If ft1: No Baseline RBBB **AND** ft2: Absence of New ECG Changes
Then Early Discharge

Rule 2: 24 h Inpatient Monitoring
If ft3: Baseline RBBB **OR** ft5: New-onset RBBB **OR** ft6: New-onset LBBB **AND** ft8: 130 ms < QRS < 160 ms
Then 24 h Inpatient Monitoring

Rule 3: 48 h Inpatient Monitoring
If ft4: Baseline LBBB **OR** ft6: New-onset LBBB **AND** ft7: Post balloon dilatation **OR** ft9: Prolongation of PR $>$ 20 ms
Then 48 h Inpatient Monitoring

Rule 4: >48 h Monitoring
If ft11: Baseline Hypertension **AND** ft12: Diabetes Mellitus **AND** ft13: Male Sex **OR** ft14: Age significant factor
Then > 48 h Monitoring

Rule 5: 24 h Inpatient Monitoring
If ft10: QRS $>$ 160 ms**OR** ft3: Baseline RBBB
Then 24 h Inpatient Monitoring

Rule 6: 48 h Inpatient Monitoring
If ft3: Baseline RBBB **OR** ft4: Baseline LBBB **OR** ft5: New-onset RBBB **OR** ft6: New-onset LBBB **AND** ft9: Prolongation of PR $>$ 20 ms **OR** ft14: Age $>$ 80
Then 48 h Inpatient Monitoring

Although ANFIS offers a strong basis for interpretable models, the model's transparency and interpretability can be further improved by utilizing XAI approaches, particularly the SHAP and LIME libraries. With the help of XAI technologies, decision-making may be understood at greater depth and more clearly, enabling patients to grasp the results and professionals. Therefore, to identify the effectiveness of our method, we used the SHAP and LIME libraries of XAI frameworks as our primary tools for data analysis. While LIME offers a local approximation of the model's behavior around particular predictions of interest, SHAP prioritizes the significance of each characteristic in the model's decision-making process. The SHAP-based analysis shows the average impact of each feature in Figure 7a. Remarkably, the most significant characteristic in determining which individuals need to be monitored for possible pacemaker implantation is the baseline RBBB. The patient may need a PPMI within two days due to the presence of baseline Left Bundle Branch Block (LBBB) and the recent emergence of RBBB and LBBB, which indicate a higher risk. These results support the theoretical relationships shown in Table 2 and are reflected in the Fuzzy rules, indicating successful model training. Figure 7b shows how, in a particular scenario, the model predicts with an 85% chance that PPMI will be required within 24 h and with probabilities of 9% and 2% for requirements beyond 48 h, respectively. Considering the abnormality in the duration of QRS and the existence of new-onset LBBB, this validates the accuracy of the model predictions. This XAI-based analysis effectively converts Machine Learning from a black box dictating prediction into a consultation tool by improving the model's transparency and assisting doctors in their decision-making.

Figure 7. Visualization of important features in decision-making with the proposed model through XAI techniques. (**a**) Impact of features on the proposed model output prediction based on SHAP values. (**b**) Impact of features on model output prediction for an individual sample based on LIME values.

3.3. Model Limitations

Although our model is novel in that it uses quantum-enhanced approaches for PPMI prediction post-TAVR, it has several drawbacks that may restrict its wider use and effectiveness. First and foremost, implementing it in a noisy quantum environment presents many difficulties. Quantum noise and decoherence can severely impact our model's accuracy and dependability.

Furthermore, it is not entirely established whether our approach can be applied to other datasets. Different medical centers may have different clinical and demographic data, which could cause differences in the model's performance since the validation we are currently performing depends mostly on data that is exclusive to our original experimental design.

It is noticed that our method involved projecting the knowledge insights onto the dataset that we had obtained from [35]. Therefore, the potential for the introduction of expert knowledge bias is another significant constraint. Predictions may be skewed by the model's reliance on expert inputs for feature selection and parameter tuning, especially if the expert data are biased toward particular demographic or clinical outcomes or do not

fairly represent larger patient populations. This might make the model less applicable in a variety of clinical contexts and could have an impact on decision-making procedures that depend on the model's outputs.

3.4. Future Works

To improve our model's performance and flexibility across a range of clinical contexts, we plan on conducting more in-depth research on the application of transfer learning techniques in the future, which entails the following:

- Cross-Domain Adaptation: To test and improve our model, we will use a variety of datasets from various medical centers. These datasets may have distinct feature relevancies and distributions. This modification will increase the model's resilience to various clinical data features and enable us to apply the model more broadly.
- Feature Representation Learning: We seek to discover and encode more profound, abstract clinical data representations that apply to various tasks using sophisticated feature representation approaches. This will improve the model's capacity to extract valuable information from hidden data.
- Task-Specific Tuning: Modifications to the model may be necessary for every clinical task. To optimize our model for particular tasks—like forecasting additional cardiovascular events—we intend to investigate ways to use less labeled data from the target domain while preserving the information we acquired from the source domain.

Additionally, there is more promise in quantum computing than we currently realize. We intend to investigate the following:

- Advanced Quantum Algorithms: Investigation of algorithms for complicated healthcare dataset optimization, such as Variational Quantum Eigensolvers (VQEs) and Quantum Annealing.
- Hybrid Quantum-Classical Models: These models have the potential to combine the benefits of both classical and quantum computing, providing the resilience and stability of classical computing with the speed and parallelism of quantum computing.

4. Conclusions

In this paper, we studied a novel method to enhance the prediction of PPMI after TAVR by integrating QACO with the ANFIS. Especially for high-dimensional and unbalanced datasets commonly found in healthcare, our methodology dramatically improves feature selection and parameter optimization efficiency by leveraging quantum computing to solve the computational hurdles inherent in standard methodologies.

Our results demonstrate significant gains in accuracy, precision, recall, and F1 score, indicating that the proposed quantum-enhanced ANFIS model works significantly better than current approaches. While the XAI techniques enhance the transparency and interpretability of our model, enabling better clinical decision-making, expert knowledge integration guarantees the clinical relevance of our predictions.

Despite its strength, our model could raise concerns about its stability and reliability within the noisy quantum environment. Furthermore, one needs to carefully consider and mitigate potential generalization issues of the model across different datasets and possible biases introduced by expert knowledge in the model.

Therefore, our future investigations will improve our method's generality across a range of datasets from different clinical centers. Using transfer learning strategies is a promising approach. These will enhance our model's feature selection process and better utilize expert knowledge. With this approach, we can make clinical data more resilient and flexible by utilizing more perceptive and profound features. In light of this development, our quantum-enhanced ANFIS model can be customized to meet the unique requirements of various patient populations and healthcare facilities. Furthermore, we plan to explore more sophisticated quantum algorithms in the future, such as Quantum Annealing and VQE, which are well-suited for optimizing intricate healthcare datasets. To

improve computational accuracy and efficiency, we will also investigate hybrid quantum-classical models, which combine the speed and parallelism of quantum computing with the robustness and stability of classical computing.

Author Contributions: Conceptualization, L.T.; methodology, L.T.; software, L.T.; validation, L.T. and J.Y.; formal analysis, L.T.; investigation, L.T. and J.Y.; writing—original draft preparation, L.T.; writing—review and editing, L.T. and J.Y.; visualization, L.T.; supervision, J.Y. All authors have read and agreed to the published version of the manuscript.

Funding: This research received no external funding.

Data Availability Statement: The data that support the findings of this study are available from the corresponding author upon reasonable request.

Conflicts of Interest: The authors declare no conflicts of interest.

Abbreviations

The following abbreviations are used in this manuscript:

TAVR	Transcatheter Aortic Valve Replacement
PPMI	Permanent Pacemaker Implantation
QACO	Quantum Ant Colony Optimization
ANFIS	Adaptive Neuro-Fuzzy Inference System
XAI	eXplainable Artificial Intelligence
ML	Machine Learning
SLR	Simple Logistic Regression
LWL	Locally Weighted Learner
GBM	Gradient Boosting Machine
ECG	Electrocardiogram
SVI	Stroke Volume Index
RBBB	Right Bundle Branch Block
THV	Transcatheter Heart Valve
BP	Backpropagation
PSO	Particle Swarm Optimization
ACO	Ant Colony Optimization
BWOA	Black Widow Optimization Algorithm
GA	Genetic Algorithm
LAFB	Left Anterior Fascicular Block
LVOT	Left Ventricular Outflow Tract
QML	Quantum Machine Learning
SHAP	SHapley Additive exPlanations
LIME	Local Interpretable Model-Agnostic Explanations
LSE	Least Squares Estimation
NISQ	Noisy Intermediate-Scale Quantum
LBBB	Left Bundle Branch Block
VQE	Variational Quantum Eigensolvers

References

1. Tsushima, T.; Al-Kindi, S.; Nadeem, F.; Attizzani, G.F.; Elgudin, Y.; Markowitz, A.; Costa, M.A.; Simon, D.I.; Arruda, M.S.; Mackall, J.A.; et al. Machine Learning Algorithms for Prediction of Permanent Pacemaker Implantation After Transcatheter Aortic Valve Replacement. *Circ. Arrhythmia Electrophysiol.* **2021**, *14*, e008941. [CrossRef]
2. Agasthi, P.; Ashraf, H.; Pujari, S.H.; Girardo, M.; Tseng, A.; Mookadam, F.; Venepally, N.; Buras, M.R.; Abraham, B.; Khetarpal, B.K.; et al. Prediction of permanent pacemaker implantation after transcatheter aortic valve replacement: The role of machine learning. *World J. Cardiol.* **2023**, *15*, 95–105. [CrossRef]
3. Truong, V.T.; Beyerbach, D.; Mazur, W.; Wigle, M.; Bateman, E.; Pallerla, A.; Ngo, T.N.; Shreenivas, S.; Tretter, J.T.; Palmer, C.; et al. Machine learning method for predicting pacemaker implantation following transcatheter aortic valve replacement. *Pacing Clin. Electrophysiol.* **2021**, *44*, 334–340. [CrossRef] [PubMed]
4. Pandey, A.C.; Nichani, A.; Pelter, M.; Ng, D.; Jaravata, A.; Duncan, Z.; Suresh, S.; Mehta, S.; Stinis, C.; Bhavnani, S.; et al. Machine learning for prediction of pacemaker after tavr in patients with low stroke volume index. *J. Am. Coll. Cardiol.* **2021**, *77*, 1182. [CrossRef]

5. Qi, Y.; Lin, X.; Pan, W.; Zhang, X.; Ding, Y.; Chen, S.; Zhang, L.; Zhou, D.; Ge, J. A prediction model for permanent pacemaker implantation after transcatheter aortic valve replacement. *Eur. J. Med. Res.* **2023**, *8*, 262. [CrossRef]
6. Mauri, V.; Reimann, A.; Stern, D.; Scherner, M.; Kuhn, E.; Rudolph, V.; Rosenkranz, S.; Eghbalzadeh, K.; Friedrichs, K.; Wahlers, T.; et al. Predictors of permanent pacemaker implantation after transcatheter aortic valve replacement with the SAPIEN 3. *JACC Cardiovasc. Interv.* **2016**, *9*, 2200–2209. [CrossRef] [PubMed]
7. Mahajan, S.; Gupta, R.; Malik, A.H.; Mahajan, P.; Aedma, S.K.; Aronow, W.S.; Mehta, S.S.; Lakkireddy, D.R. Predictors of permanent pacemaker insertion after TAVR: A systematic review and updated meta-analysis. *J. Cardiovasc. Electrophysiol.* **2021**, *32*, 1411–1420. [CrossRef]
8. Sugiyama, Y.; Miyashita, H.; Yokoyama, H.; Ochiai, T.; Shishido, K.; Jalanko, M.; Yamanaka, F.; Vähäsilta, T.; Saito, S.; Laine, M.; et al. Risk Assessment of Permanent Pacemaker Implantation After Transcatheter Aortic Valve Implantation in Patients With Preexisting Right Bundle Branch Block. *Am. J. Cardiol.* **2024**, *213*, 151–160. [CrossRef]
9. Feistritzer, H.; Stachel, G.; Kurz, T.; Eitel, I.; Marquetand, C.; Abdel-Wahab, M.; Desch, S.; Thiele, H. Predictors of permanent pacemaker implantation after transcatheter aortic valve implantation-Results from the SOLVE-TAVI trial. *Eur. Heart J.* **2023**, *44*, ehad655.1669. [CrossRef]
10. Nwaedozie, S.; Zhang, H.; Mojarrab, J.N.; Sharma, P.; Yeung, P.; Umukoro, P.; Soodi, D.; Gabor, R.; Anderson, K.; Garcia-Montilla, R. Novel predictors of permanent pacemaker implantation following transcatheter aortic valve replacement. *World J. Cardiol.* **2023**, *15*, 582. [CrossRef] [PubMed]
11. Zhang, J.; Chi, C.; Tian, S.; Zhang, S.; Liu, J. Predictors of Permanent Pacemaker Implantation in Patients After Transcatheter Aortic Valve Replacement in a Chinese Population. *Front. Cardiovasc. Med.* **2022**, *8*, 743257. [CrossRef] [PubMed]
12. Rmilah, A.A.A.; Al-Zu'bi, H.; Haq, I.U.; Yagmour, A.H.; Jaber, S.A.; Alkurashi, A.K.; Qaisi, I.; Kowlgi, G.N.; Cha, Y.M.; Mulpuru, S.; et al. Predicting permanent pacemaker implantation following transcatheter aortic valve replacement: A contemporary meta-analysis of 981,168 patients. *Heart Rhythm O_2* **2022**, *3*, 385–392. [CrossRef]
13. Ullah, W.; Zahid, S.; Zaidi, S.R.; Sarvepalli, D.; Haq, S.; Roomi, S.; Mukhtar, M.; Khan, M.A.; Gowda, S.N.; Ruggiero, N.; et al. Predictors of permanent pacemaker implantation in patients undergoing transcatheter aortic valve replacement-a systematic review and meta-analysis. *J. Am. Heart Assoc.* **2021**, *10*, e020906. [CrossRef] [PubMed]
14. Tsushima, T.; Nadeem, F.; Al-Kindi, S.; Clevenger, J.R.; Bansal, E.J.; Wheat, H.L.; Kalra, A.; Attizzani, G.F.; Elgudin, Y.; Markowitz, A.; et al. Risk prediction model for cardiac implantable electronic device implantation after transcatheter aortic valve replacement. *Clin. Electrophysiol.* **2020**, *6*, 295–303. [CrossRef] [PubMed]
15. Veulemans, V.; Frank, D.; Seoudy, H.; Wundram, S.; Piayda, K.; Maier, O.; Jung, C.; Polzin, A.; Frey, N.; Kelm, M.; et al. New insights on potential permanent pacemaker predictors in TAVR using the largest self-expandable device. *Cardiovasc. Diagn. Ther.* **2020**, *10*, 1816. [CrossRef]
16. Kiani, S.; Kamioka, N.; Black, G.B.; Lu, M.L.R.; Lisko, J.C.; Rao, B.; Mengistu, A.; Gleason, P.T.; Stewart, J.P.; Caughron, H.; et al. Development of a risk score to predict new pacemaker implantation after transcatheter aortic valve replacement. *JACC Cardiovasc. Interv.* **2019**, *12*, 2133–2142. [CrossRef]
17. Pellegrini, C.; Husser, O.; Kim, W.K.; Holzamer, A.; Walther, T.; Rheude, T.; Mayr, N.P.; Trenkwalder, T.; Joner, M.; Michel, J.; et al. Predictors of need for permanent pacemaker implantation and conduction abnormalities with a novel self-expanding transcatheter heart valve. *Rev. Esp. Cardiol. (Engl. Ed.)* **2019**, *72*, 145–153. [CrossRef]
18. Vejpongsa, P.; Zhang, X.; Bhise, V.; Kitkungvan, D.; Shivamurthy, P.; Anderson, H.V.; Balan, P.; Nguyen, T.C.; Estrera, A.L.; Dougherty, A.H.; et al. Risk prediction model for permanent pacemaker implantation after transcatheter aortic valve replacement. *Struct. Heart* **2020**, *2*, 328–335. [CrossRef]
19. Maeno, Y.; Abramowitz, Y.; Kawamori, H.; Kazuno, Y.; Kubo, S.; Takahashi, N.; Mangat, G.; Okuyama, K.; Kashif, M.; Chakravarty, T.; et al. A highly predictive risk model for pacemaker implantation after TAVR. *JACC Cardiovasc. Imaging* **2017**, *10*, 1139–1147. [CrossRef]
20. Nazif, T.M.; Dizon, J.M.; Hahn, R.T.; Xu, K.; Babaliaros, V.; Douglas, P.S.; El-Chami, M.F.; Herrmann, H.C.; Mack, M.; Makkar, R.R.; et al. Predictors and clinical outcomes of permanent pacemaker implantation after transcatheter aortic valve replacement: the PARTNER (Placement of AoRtic TraNscathetER Valves) trial and registry. *JACC Cardiovasc. Interv.* **2015**, *8*, 60–69. [CrossRef]
21. Hosseinzadeh, M.; Yoo, J.; Ali, S.; Lansky, J.; Mildeova, S.; Yousefpoor, M.S.; Ahmed, O.H.; Rahmani, A.M.; Tightiz, L. A fuzzy logic-based secure hierarchical routing scheme using firefly algorithm in Internet of Things for healthcare. *Sci. Rep.* **2023**, *13*, 11058. [CrossRef] [PubMed]
22. Şener, R.; Koç, M.A.; Ermiş, K. Hybrid ANFIS-PSO algorithm for estimation of the characteristics of porous vacuum preloaded air bearings and comparison performance of the intelligent algorithm with the ANN. *Eng. Appl. Artif. Intell.* **2024**, *128*, 107460. [CrossRef]
23. Aghelpour, P.; Graf, R.; Tomaszewski, E. Coupling ANFIS with ant colony optimization (ACO) algorithm for 1-, 2-, and 3-days ahead forecasting of daily streamflow, a case study in Poland. *Environ. Sci. Pollut. Res.* **2023**, *30*, 56440–56463. [CrossRef] [PubMed]
24. Tightiz, L.; Yang, H. An Intelligent System for Power Transformer Fault Diagnosis. KR Patent 102495822, 31 January 2023.
25. Tightiz, L.; Nasab, M.A.; Yang, H.; Addeh, A. An intelligent system based on optimized ANFIS and association rules for power transformer fault diagnosis. *ISA Trans.* **2020**, *103*, 63–74. [CrossRef] [PubMed]

26. Ray, R.; Choudhary, S.S.; Roy, L.B.; Kaloop, M.R.; Samui, P.; Kurup, P.U.; Ahn, J.; Hu, J.W. Reliability analysis of reinforced soil slope stability using GA-ANFIS, RFC, and GMDH soft computing techniques. *Case Stud. Constr. Mater.* **2023**, *18*, e01898. [CrossRef]
27. Barker, M.; Sathananthan, J.; Perdoncin, E.; Devireddy, C.; Keegan, P.; Grubb, K.; Pop, A.M.; Depta, J.P.; Rai, D.; Abtahian, F.; et al. Same-Day Discharge Post–Transcatheter Aortic Valve Replacement During the COVID-19 Pandemic: The Multicenter PROTECT TAVR Study. *Cardiovasc. Interv.* **2022**, *15*, 590–598.
28. Gupta, R.; Mahajan, S.; Mehta, A.; Nyaeme, M.; Mehta, N.A.; Cheema, A.; Khanal, L.; Malik, A.H.; Aronow, W.S.; Vyas, A.V.; et al. Next-day discharge vs. early discharge after transcatheter aortic valve replacement: Systematic review and meta-analysis. *Curr. Probl. Cardiol.* **2022**, *47*, 100998. [CrossRef] [PubMed]
29. Bansal, A.; Garg, C.; Hariri, E.; Kassis, N.; Mentias, A.; Krishnaswamy, A.; Kapadia, S.R. Machine learning models predict total charges and drivers of cost for transcatheter aortic valve replacement. *Cardiovasc. Diagn. Ther.* **2022**, *12*, 464. [CrossRef]
30. Ullah, U.; Garcia-Zapirain, B. Quantum Machine Learning Revolution in Healthcare: A Systematic Review of Emerging Perspectives and Applications. *IEEE Access* **2024**, *12*, 11423–11450. [CrossRef]
31. Mahdavi, Z.; Samavat, T.; Javanmardi, A.S.J.; Dashtaki, M.A.; Zand, M.; Nasab, M.A.; Nasab, M.A.; Padmanaban, S.; Khan, B. Providing a Control System for Charging Electric Vehicles Using ANFIS. *Int. Trans. Electr. Energy Syst.* **2024**, *1*, 9921062. [CrossRef]
32. Shafique, M.A.; Munir, A.; Latif, I. Quantum Computing: Circuits, Algorithms, and Applications. *IEEE Access* **2024**, *12*, 22296–22314. [CrossRef]
33. Sarkar, M.; Pradhan, J.; Singh, A.K.; Nenavath, H. A Novel Fast Path Planning Approach for Mobile Devices using Hybrid Quantum Ant Colony Optimization Algorithm. *arXiv* **2023**, arXiv:2310.17808.
34. Selma, B.; Chouraqui, S.; Abouaïssa, H. Optimization of ANFIS controllers using improved ant colony to control an UAV trajectory tracking task. *SN Appl. Sci.* **2020**, *2*, 878. [CrossRef]
35. Tichelbäcker, T.; Bergau, L.; Puls, M.; Friede, T.; Mütze, T.; Maier, L.S.; Frey, N.; Hasenfuß, G.; Zabel, M.; Jacobshagen, C.; et al. Insights into permanent pacemaker implantation following TAVR in a real-world cohort. *PLoS ONE* **2018**, *13*, e0204503. [CrossRef] [PubMed]
36. Bhavsar, R.; Jadav, N.K.; Bodkhe, U.; Gupta, R.; Tanwar, S.; Sharma, G.; Bokoro, P.N.; Sharma, R. Classification of potentially hazardous asteroids using supervised quantum machine learning. *IEEE Access* **2023**, *11*, 75829–75848. [CrossRef]